Eur. Phys. J. B **23**, 441–448 (2001)

**THE EUROPEAN PHYSICAL JOURNAL B**

EDP Sciences


# Soft X-ray magnetic circular dichroism in Fe and $Fe_{0.50}Co_{0.48}V_{0.02}$ films: quantitative analysis of transmission

O. Zaharko[1,a], A. Cervellino[2], H.-Ch. Mertins[3], H. Grimmer[1], F. Schäfers[3], and D. Arvanitis[4]

[1] Laboratory for Neutron Scattering, ETH&PSI, 5232 Villigen PSI, Switzerland
[2] Laboratory of Crystallography, ETH Zentrum, Sonnegstrasse 5, 8092 Zurich, Switzerland
[3] BESSY, Albert-Einstein-Strasse 15, 12489 Berlin, Germany
[4] Department of Physics, Uppsala University, Box 530, 75121 Uppsala, Sweden

Received 15 August 2000 and Received in final form 11 June 2001

**Abstract.** Magnetic circular dichroism (MCD) in X-ray absorption has been measured at the $L_{2,3}$ edges of Fe in *ex-situ* grown Fe and $Fe_{0.50}Co_{0.48}V_{0.02}$ films by means of the transmission method. A new approach is developed for fitting the observed transmittance, which describes the resonance lineshapes as (generalized) Fano profiles. Analytical integration of each single resonance allows a more reliable determination of the orbital and spin magnetic moments based on the MCD sum rules. The results are consistent with an increase of the Fe spin and orbital magnetic moment in Fe-Co alloys as obtained by other experiments and band structure calculations.

**PACS.** 78.70.Dm X-ray absorption spectra – 87.64.Ni Optical absorption, magnetic circular dichroism, fluorescence spectroscopy

## 1 Introduction

X-ray magnetic circular dichroism (MCD) in X-ray absorption spectra (XAS) has become a powerful tool to study magnetism on the atomic scale. To obtain the values of magnetic moments one must integrate the absorption lines separately [1,2]. This task is difficult as the line profiles are complex and partly overlapping, and the background is also structured. Furthermore, experimental distortions (saturation [3,4], leakage [5]) are to be taken into account to achieve an acceptable precision.

This contribution presents a new method for quantitative data analysis of XAS and MCD. The experimental absorption profiles have been analytically approximated, including background and experimental distortions. This allowed to integrate analytically and separately each resonance, with automatic background subtraction. Making use of the angular dependence of XAS, we determine a) – the absolute degree of circular polarization of the incoming radiation, b) – the absolute absorption cross sections of relatively thick films[1], c) – the orbital $m_L$ and spin $m_S$ components of the magnetic moment applying the magneto-optic sum rules [1,2].

This procedure has been tested on $Fe_{0.50}Co_{0.48}V_{0.02}$ and Fe films. The obtained magnetic moments confirm the theoretical predictions on enhancement of the Fe spin component in Fe-Co alloys.

## 2 Experimental details

The 20 nm Fe and 30 nm $Fe_{0.50}Co_{0.48}V_{0.02}$ films[2] were deposited on 500 nm thick $Si_3N_4$ membranes by dc magnetron sputtering. The films are polycrystalline with the in-plane grain size of 10–20 nm. X-ray absorption spectra were measured in transmission at the Fe $L_{2,3}$ edges at the elliptically polarizing undulator beamline UE56/1 PGM [6] at BESSY II using the soft X-ray polarimeter [7]. The energy resolution was set to $E/\Delta E \approx 1600$, the degree of circular polarization to 0.85. The spectra were taken flipping between the two opposite directions of a saturation magnetic field (±500 Oe) applied parallel to the film surface. The transmitted light was detected by measuring the total current of a GaAsP photodiode. The direct beam intensity $\mathbb{I}_0$ was measured separately with the same detector. All measured spectra were normalized to $\mathbb{I}_0$ and to the electron current in the storage ring.

Data were acquired for several incidence angles in the range $45^o \leq \theta \leq 90^o$. The transmittances measured at $\theta = 50^o$ are shown in figure 1 together with the corresponding asymmetry $\mathbb{A}_m = (\mathbb{T}^+ - \mathbb{T}^-) / (\mathbb{T}^+ + \mathbb{T}^-)$.

[a] e-mail: Oksana.Zaharko@psi.ch

[1] *Ex-situ* grown transmission samples with several dozens nm thickness.

[2] Small amounts of V increase homogeneity of the film.

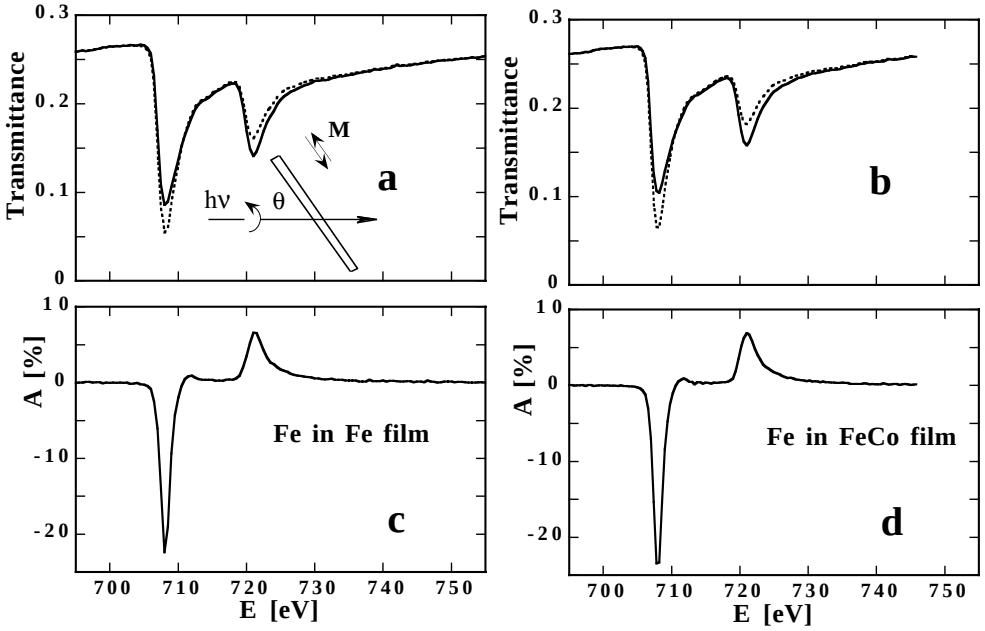


**Fig. 1.** Measured transmittances at the Fe $L_{3,2}$ edges ($\theta = 50^{\circ}$) and corresponding asymmetry $\mathbb{A}_m$ for the Fe (a, c) and $Fe_{0.50}Co_{0.48}V_{0.02}$ (b, d) films. Inset: experimental setup.

## 3 Model description

### 3.1 Transmittance of a magnetic film

Coherent synchrotron radiation can be considered as a coherent superposition of two circularly polarized parts having opposite handedness (helicity). Its total intensity $\mathbb{I}_0$ is the sum of the left-($\mathbb{I}_\mathrm{L}$) and right-($\mathbb{I}_\mathrm{R}$) handed circularly polarized intensities:

$$\mathbb{I}_0 = \mathbb{I}_\mathrm{L} + \mathbb{I}_\mathrm{R}. \tag{1}$$

When elliptically polarized light passes through a film with a net macroscopic magnetization, different absorption of the two components results in MCD asymmetries. The two fractions of the transmitted intensity are related to the fractions of the incoming light:

$$\mathbb{I}_\pm = \mathbb{I}_\mathrm{L} \exp(\mathcal{L}) + \mathbb{I}_\mathrm{R} \exp(\mathcal{R}) \tag{2}$$

with $\mathcal{L}$ and $\mathcal{R}$:

$$\mathcal{L} = -\left( \frac{\mu\, r}{\sin\theta} \pm \frac{\Delta\mu\, r}{\tan\theta} \right) \tag{3}$$

$$\mathcal{R} = -\left( \frac{\mu\, r}{\sin\theta} \mp \frac{\Delta\mu\, r}{\tan\theta} \right) \tag{4}$$

where $\pm$ denotes parallel or antiparallel coupling of the film magnetization $\boldsymbol{M}$ and the photon helicity. The quantities $\mu$ and $\Delta\mu$ are the atomic absorption coefficient and its dichroic contribution, $r$ is the film thickness, $\theta$ the angle of incidence relative to the film surface (Fig. 1 inset).

In real experimental conditions equations (1, 2) are not strictly fulfilled. The possible distortions are [5]: scattering from the sample, higher harmonics, stray and unpolarized light, thickness effects and radiation leakage. We found that the most important distortion is radiation leakage due to nonuniformity of the sample (*e.g.* microholes). Its magnitude (possibly large) cannot be estimated *a priori*, so it needs to be analyzed. The transmitted intensity ($\mathbb{I}'_\pm$) is then split into the leaking (not attenuated) part $X\mathbb{I}_0$ and the attenuated part $(1-X)\mathbb{I}_\pm$:

$$\mathbb{I}'_\pm = X\mathbb{I}_0 + (1-X)\mathbb{I}_\pm \tag{5}$$

where $X$ is the 'leaking fraction', or the effective fractional area of the holes in the sample[3]. The transmittance $\mathbb{T}$ is then written as

$$\mathbb{T}_\pm = X + (1-X)\left(\mathbb{P}_\mathrm{L} \exp(\mathcal{L}) + \mathbb{P}_\mathrm{R} \exp(\mathcal{R})\right) \tag{6}$$

where $\mathbb{P}_\mathrm{L} = \mathbb{I}_\mathrm{L}/\mathbb{I}_0$ and $\mathbb{P}_\mathrm{R} = \mathbb{I}_\mathrm{R}/\mathbb{I}_0$ are the intensity fractions of the left- and right- handed circularly polarized light in the incoming beam. If the radiation is coherent, $\mathbb{P}_\mathrm{L} + \mathbb{P}_\mathrm{R} = 1$ and the normalized Stokes parameter $S_3$ [8] of the incoming beam is

$$S_3 = \left(\mathbb{P}_\mathrm{R} - \mathbb{P}_\mathrm{L}\right) / \left(\mathbb{P}_\mathrm{R} + \mathbb{P}_\mathrm{L}\right).$$

[3] Empirically we found that $X \approx k \sin(\theta)$, where $k$ can be as large as 0.3. This angular dependence allows us to decouple and correct also severe leakages, as verified with several data sets.

Finally, we can define the average transmittance

$$\mathbb{T}_A \equiv \frac{\mathbb{T}_+ + \mathbb{T}_-}{2} = X + (1-X)\exp\left(\frac{-\mu r}{\sin\theta}\right)\cosh\left(\frac{\Delta\mu r}{\tan\theta}\right) \tag{7}$$

and the differential transmittance

$$\mathbb{T}_D \equiv \frac{\mathbb{T}_+ - \mathbb{T}_-}{2} = S_3(1-X)\exp\left(\frac{-\mu r}{\sin\theta}\right)\sinh\left(\frac{\Delta\mu r}{\tan\theta}\right). \tag{8}$$

In Section 3.2 we will give an effective analytical expression of the energy dependence of $\mu r(E)$ and $\Delta\mu r(E)$. Equations (7, 8) will be used in Section 4 to fit the experimental transmittances.

### 3.2 Parametrization and integration of $\mu r$ and $\Delta\mu r$

The attenuations $\mu r(E)$ and $\Delta\mu r(E)$ represent the photoabsorption (XAS) and its associated dichroism (MCD) and contain the element-specific and component-resolved information on the magnetic moments in the studied films.

The spin and orbital magnetic moments can be determined from the line integrals of $\mu r$ and $\Delta\mu r$ applying the magneto-optical sum rules [1,2]. Assuming only dipole transitions and neglecting the contribution of the magnetic dipole operators, the sum rules yield

$$m_{\mathrm{L}} = -\frac{4}{3}n\frac{\int_{\mathrm{L}_2}\Delta\mu r\,\mathrm{d}E \;+\; \int_{\mathrm{L}_3}\Delta\mu r\,\mathrm{d}E}{\int_{\mathrm{L}_2}\mu r\,\mathrm{d}E \;+\; \int_{\mathrm{L}_3}\mu r\,\mathrm{d}E} \tag{9}$$

$$m_{\mathrm{S}} = -2n\frac{\int_{\mathrm{L}_3}\Delta\mu r\,\mathrm{d}E - 2\int_{\mathrm{L}_2}\Delta\mu r\,\mathrm{d}E}{\int_{\mathrm{L}_2}\mu r\,\mathrm{d}E \;+\; \int_{\mathrm{L}_3}\mu r\,\mathrm{d}E}\,. \tag{10}$$

The accuracy of the absolute moment determination is very sensitive to errors in the integration and to the number $n$ of $3d$ band holes per atom.

The integration of both the $\Delta\mu r(E)$ (MCD) and $\mu r(E)$ (XAS) spectra is commonly performed according to the semi-empirical recipe given in [9]. There the line integrals are evaluated graphically. The XAS lines corresponding to the $\mathrm{L}_2$ and $\mathrm{L}_3$ transitions from the $2p$ to the $3d$ bands are approximated by $\delta$-peaks; the background is assumed to consist of a linear part and a double step function, which models the transitions into the $s$ conduction continuum. Intrinsic (Lorentzian) and instrumental (Gaussian) broadening are assumed. For the graphical integration of the single lines, it is necessary to evaluate very precisely background level, slope and height of the double-step. Furthermore, the $\mathrm{L}_2$ and $\mathrm{L}_3$ lines overlap significantly, making it awkward to choose a cutoff point. In addition, evident asymmetries in the peak shapes cannot be reproduced by this simple model.

We evolved this approach in two ways: a) the line profiles $\Delta\mu r(E)$, $\mu r(E)$ and background are represented by a simple analytical function of $E$, with all its free parameters evaluated by data fitting; b) asymmetric Fano lineshapes are used. Our choice of profiles is based on criteria of simplicity and functionality. We do not automatically assume the corresponding physical effect.

In the simplest case (isolated resonance interacting with a single continuum) the Fano lineshape is usually written in the form [10,11]

$$\mathfrak{F}(E) = \sigma(q+\epsilon)^2 \,/\, \left(1+\epsilon^2\right) \tag{11}$$

with $\sigma$ – intrinsic background, $q$ – asymmetry parameter, $\epsilon = \left(E - E^0\right)/w$, $E^0$ – line center, $w$ – intrinsic line width. Neglecting a constant term, this can be rewritten as a linear combination of a Lorentzian profile with an odd-parity asymmetry term

$$\mathfrak{F}(E) = \frac{V}{\pi(1+\epsilon^2)} + \frac{AV\epsilon}{\pi(1+\epsilon^2)}\,. \tag{12}$$

The independent parameters are now ($V$, $A$, $w$, $E^0$) instead of ($\sigma$, $q$, $w$, $E^0$)[4]. $A$ is the relative weight of the asymmetry term. The latter integrates to zero, so that $V = \int_{-\infty}^{+\infty}\mathfrak{F}(E)\,\mathrm{d}E$. This form is unchanged for partly overlapping multiple profiles as the $\mathrm{L}_2$, $\mathrm{L}_3$ lines, except for a linear background term [13]. The $\mu r(E)$ and $\Delta\mu r(E)$ spectra can be written as a sum of two profiles $\mathfrak{F}_i(E)$. Instrumental broadening is taken into account by convolution with a normalized Gaussian function $\mathfrak{G}(E)$[5], whose width is also a free parameter. Background is represented by a linear term incorporating several contributions plus a smoothed double-step representing the density of unoccupied $s$ states. Smoothing of each step is achieved by convolution with the Lorentzian part of the corresponding line and with the same Gaussian $\mathfrak{G}$. The branching ratio 2:1 between the step heights is kept fixed.

The advantages of the described approach are straightforward. The functions $\mu r(E)$ and $\Delta\mu r(E)$ are simply parametrized, and the line integrals are determined directly as profile parameters. This makes it possible to develop a self-calibrating automatized procedure, which based on the averaged and differential transmittances refines the parameters of interest and, finally, calculates the magnetic moments $m_{\mathrm{L}}$ and $m_{\mathrm{S}}$. Further details of the refinement procedure are given in the Appendix.

## 4 Results and discussion

### 4.1 Results of refinement

The $\mathbb{T}_A$ and $\mathbb{T}_D$ values (*cf.* Eqs. (7,8)) obtained from the measured data for the Fe and $\mathrm{Fe_{0.50}Co_{0.48}V_{0.02}}$ films were fitted by the described approach. The quality of the fits is very good both from visual inspection (Fig. 2) and from the statistical parameters (final goodness-of-fit $\mathrm{GoF} = 9.0\times10^{-6}$ for the Fe film and $\mathrm{GoF} = 8.9\times10^{-6}$ for the $\mathrm{Fe_{0.50}Co_{0.48}V_{0.02}}$ film). The final parameters are listed in Table 1.

[4] This is essentially the 'Shore parametrization' [12].

[5] This does not affect the values of the line integrals.

**Table 1.** Results of refinement of the Fe $L_{3,2}$ absorption spectra in the Fe and $Fe_{0.50}Co_{0.48}V_{0.02}$ films. The symbols denote: $E^0_{L_i}$ — line centers [eV], $w_{L_i}$ — intrinsic linewidths [eV], $A_{L_i}$ — asymmetry parameters, $V_{L_i}$ — edge integrals, $S_3$ — degree of circular polarization, $s$ — height of the step above the resonances.

| | Fe film | | $Fe_{0.50}Co_{0.48}V_{0.02}$ film | |
|---|---|---|---|---|
| | $\mu r$ | $\Delta\mu r$ | $\mu r$ | $\Delta\mu r$ |
| $E^0_{L_3}$ | 707.850±0.004 | 708.20±0.03 | 707.721±0.004 | 708.04±0.03 |
| $w_{L_3}$ | 1.141±0.004 | 0.56±0.02 | 1.067±0.004 | 0.56±0.02 |
| $A_{L_3}$ | 0.540±0.003 | −0.04±0.03 | 0.588±0.004 | 0.01±0.02 |
| $V_{L_3}$ | 3.347±0.009 | −0.69±0.09 | 2.753±0.008 | −0.72±0.07 |
| $E^0_{L_2}$ | 720.689±0.008 | 721.33±0.05 | 720.635±0.009 | 721.16±0.05 |
| $w_{L_2}$ | 1.35 ±0.01 | 1.39±0.08 | 1.29 ±0.01 | 1.43±0.07 |
| $A_{L_2}$ | 0.434±0.006 | 0.09±0.02 | 0.447±0.007 | 0.10±0.02 |
| $V_{L_2}$ | 1.260±0.009 | 0.42±0.06 | 0.987±0.008 | 0.44±0.05 |
| $s$ | 0.048±0.002 | | 0.045±0.002 | |
| $S_3$ | 0.84±0.10 | | 0.78±0.06 | |

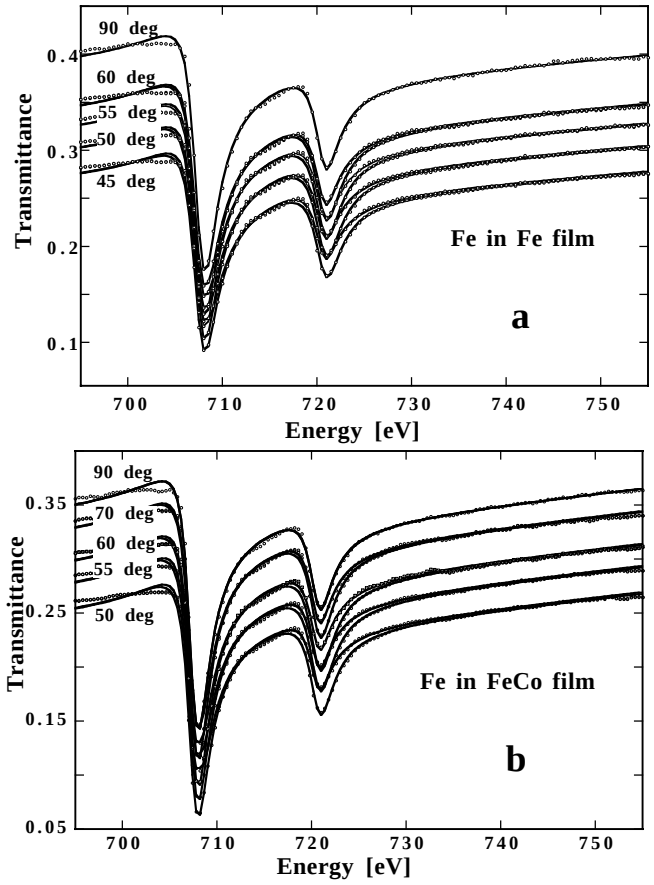


**Fig. 2.** Measured (symbols) and calculated (solid lines) transmittances at the Fe $L_{3,2}$ edges in the Fe (a) and $Fe_{0.50}Co_{0.48}V_{0.02}$ (b) films.

The refined $\mu r(E)$ and $\Delta\mu r(E)$ dependencies are plotted in Figure 3. The $\mu + \Delta\mu$ and $\mu - \Delta\mu$ values, extracted from these plots, are the absolute photoabsorption cross-sections. The resulting spin and orbital magnetic moments of Fe are $m_S = 2.2 \pm 0.2\ \mu_B$ and $m_L = 0.26 \pm 0.09\ \mu_B$ for the Fe film and $m_S = 3.4 \pm 0.2\ \mu_B$ and $m_L = 0.3 \pm 0.1\ \mu_B$ for the $Fe_{0.50}Co_{0.48}V_{0.02}$ film.

The values of the Stokes parameter $S_3$=0.84 ± 0.10 for the Fe and 0.78 ± 0.08 for the $Fe_{0.50}Co_{0.48}V_{0.02}$ films are comparable to the value 0.85 obtained during commissioning of this beamline [6].

As a result of the fit no significant radiation leakage was detected. In other cases, we could detect and quantify large leakages, and the results were confirmed by atomic force microscopy. The Gaussian broadening is found to be negligible.

To compare the results the analytical and graphical methods (Fig. 4), we performed also the graphical integration of transmittances at $\theta = 50^o$, following the established recipe of reference [9]. However, we found its application in practice, problematic. Firstly, we note that the data used for the graphical integration are complex to scale. Secondly, the MCD graphical integral (Figs. 4c, d) does not saturate at the high energy region of the measured spectra, while the analytical integration is performed over the entire absorption edge. Finally, both the spin and orbital magnetic moments obtained by the graphical procedure are systematically too low (see Tab. 2). Given the discussion of Section 3.2, we find the analytical integration more reliable for the present set of data. It is worth noting that the accuracy of the magnetic moments determination by the analytical procedure can still be increased collecting the data at additional angles

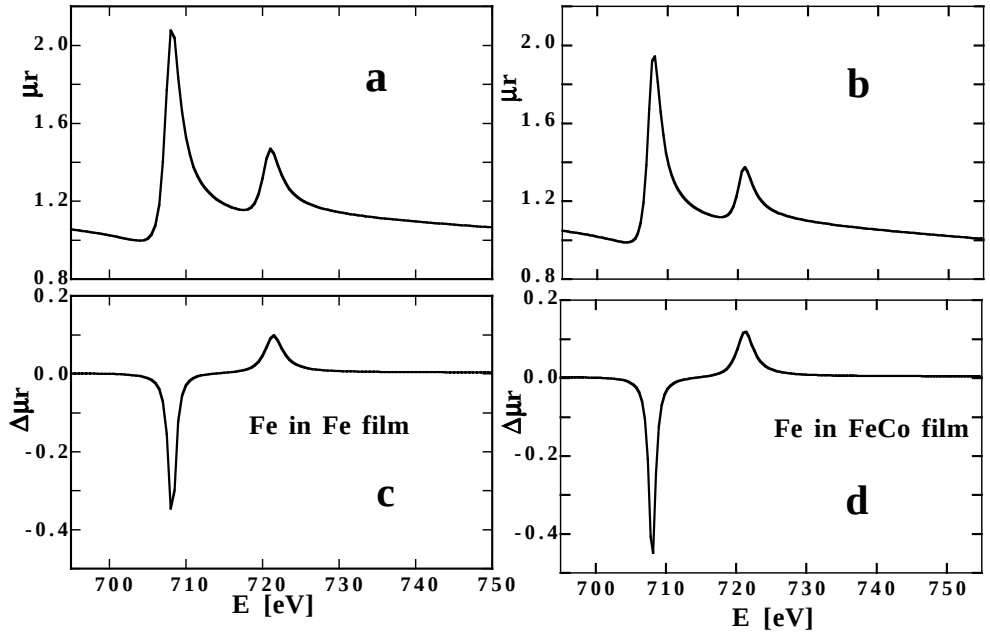


**Fig. 3.** $\mu r$ and $\Delta\mu r$ at the Fe $L_{3,2}$ edges refined using Fano profiles for the Fe (a, c) and $Fe_{0.50}Co_{0.48}V_{0.02}$ (b, d) films.

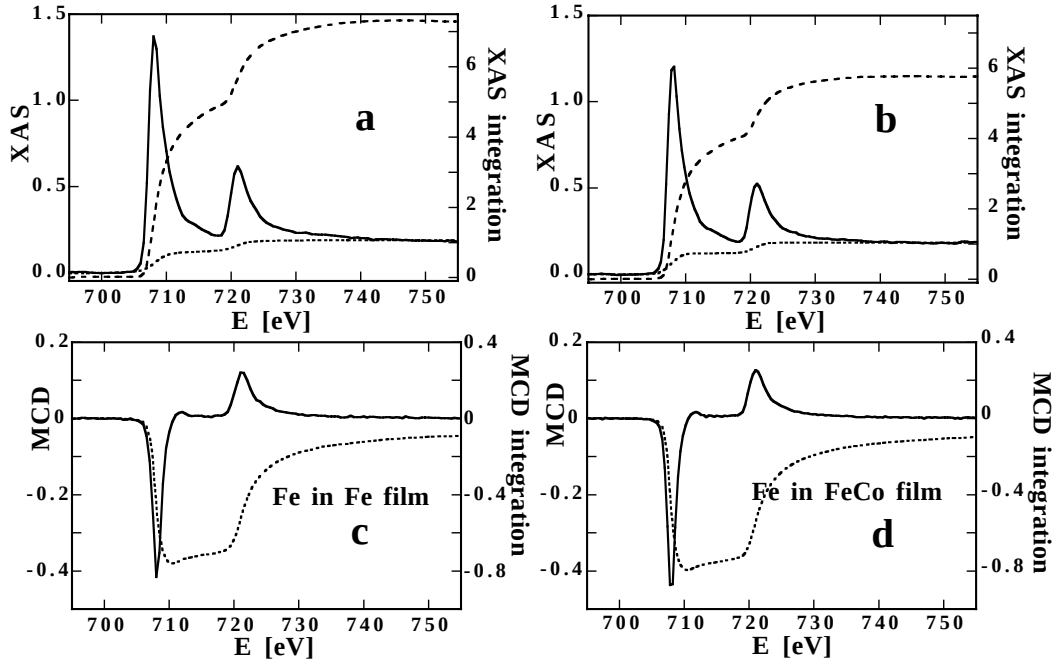


**Fig. 4.** XAS and MCD at the Fe $L_{3,2}$ edges obtained from transmittances at $\theta = 50°$ and their graphical integration (dashed lines) in the Fe (a, c) and $Fe_{0.50}Co_{0.48}V_{0.02}$ (b, d) films by the semi-empirical recipe [9].

of incidence and measuring $\mathbb{I}_0$ simultaneously with the transmittances.

### 4.2 Magnetic information on the $Fe_{0.50}Co_{0.48}V_{0.02}$ film

The information about the component resolved magnetic moment in the $Fe_{0.50}Co_{0.48}V_{0.02}$ film is of fundamental interest. It is known that bulk ordered and disordered bcc Fe-Co alloys show an anomalous increase of the Fe magnetic moment when the concentration of Co is increased above 25% [14–17]. This happens in the absence of a significant charge transfer from Fe to Co, and the Co magnetic moment remains almost constant. The band structure calculations within the local spin-density [17] as well as the spin and orbital polarized relativistic multiple scattering

**Table 2.** Orbital $m_L$, spin $m_S$ magnetic moments (in $\mu_B$/atom) of bcc Fe and their ratio $m_L/m_S$ in the Fe and $Fe_{0.50}Co_{0.48}V_{0.02}$ films obtained by the analytical integration. The values reported in literature and obtained by the graphical integration are also presented. In this work we adopt the value $n_{Fe} = 3.39$ [9].

| Structure/substrate | $m_L/m_S$ | $m_L$ | $m_S$ |
|---|---|---|---|
| | Experimental | | |
| $Fe/Si_3N_4$[a] | $0.12 \pm 0.05$ | $0.26 \pm 0.09$ | $2.2 \pm 0.2$ |
| $Fe/Si_3N_4$[b] | 0.033 | 0.058 | 1.74 |
| $Fe_{0.50}Co_{0.48}V_{0.02}/Si_3N_4$[a] | $0.12 \pm 0.03$ | $0.3 \pm 0.1$ | $3.4 \pm 0.2$ |
| $Fe_{0.50}Co_{0.48}V_{0.02}/Si_3N_4$[b] | 0.033 | 0.077 | 2.32 |
| $Fe/(C_8H_8)_n$[c] | 0.043 | 0.085 | 1.98 |
| $Fe_{0.5}Co_{0.5}$[d] | | | 3.0 |
| | Theoretical | | |
| Fe LSDA[e] | 0.018 | 0.04 | 2.22 |
| Fe OP-LSDA[e] | 0.027 | 0.06 | 2.21 |
| $Fe_{0.5}Co_{0.5}$ LSDA[f] | 0.024 | 0.065 | 2.69 |
| $Fe_{0.5}Co_{0.5}$ OP-LSDA[f] | 0.034 | 0.092 | 2.69 |
| $Fe_{0.5}Co_{0.5}$ SPR-KKR-CPA[g] | 0.020 | 0.05 | 2.5 |
| $Fe_{0.5}Co_{0.5}$ SOPR-KKR-CPA[g] | 0.032 | 0.08 | 2.5 |

[a] The present work, analytical integration.
[b] The present work, graphical integration.
[c] Values from reference [9].
[d] Values from reference [14].
[f] Values from reference [17].
[e] Values from reference [18]. LSDA and OP-LSDA stand for local spin density approximation without and with the orbital polarization term.
[g] Values from reference [16]. SPR-KKR-CPA and SOPR-KKR-CPA stand for spin and orbital polarized relativistic multiple scattering theory without and with the orbital polarization term.

(KKP-CPA) [16] theories predict that this is due to an enhancement of the Fe spin moments ($m_S = 2.5\mu_B$/Fe). Within the itinerant electron theory of magnetism this can be understood in terms of the increase of the exchange energy between the two spin sub-bands due to the mixing of Fe and Co atoms within the bcc structure, which leads to a filling of the majority band. The calculations [17] predict also an increase of the Fe orbital moment in FeCo compared to pure Fe due to band-filling effects.

Our results confirm the enhancement of the spin and orbital magnetic moments of Fe in the $Fe_{0.50}Co_{0.48}V_{0.02}$ film compared to Fe film. The total magnetic moments are in rather good agreement with results obtained by neutrons [14] (3.0 $\mu_B$/Fe for FeCo) and other MCD measurements [9] (1.98 $\mu_B$/Fe for Fe). The spin components of the magnetic moments are close to the values obtained by component resolved band structure calculations (see Tab. 2). However, there is a discrepancy between the orbital moments obtained by the analytical integration and the theory. Such a discrepancy may have two reasons. Firstly, the theoretical values may be underestimated. They are performed for "perfect" Fe and FeCo bulk materials which do not account for the presence of 2% of V atoms, disorder, surface and grain interface relaxation (grains are of order 10–20 nm in our samples). These effects will enhance the orbital moment due, among others, to a lifting of the crystal field quenching as was observed before in the case of surfaces (see for example [21]). On the other hand, our model does not account for weak features present in the $\Delta\mu r$ spectra. For example, a small positive intensity shoulder at the high-energy side of the $L_3$-edge (Fig. 2c, d) is not taken into account in our model function. It may be caused by spin polarization in the valence band [22]. As the integral $\int_{L_3+L_2} \Delta\mu r$ is obtained by subtracting the almost equal $L_2$ and $L_3$ integrals, this small feature may give up to 15% increase in the orbital moment.

We conclude that the values obtained by the analytical integration are realistic. Finally we note that up to now there is no other measurement of the orbital moment on these or similar samples. Only few MCD spectra on FeCo films were measured [19,20], but the spin and orbital magnetic moments were not determined. Therefore, the question of an increase of the orbital moment as compared to

theory should be addressed in the future by further measurements and more realistic calculations.

## 5 Conclusions

We have demonstrated a new quantitative approach to MCD X-ray absorption spectra based on the analytical integration of MCD and XAS spectra. The developed fitting procedure allowed us to determine the absolute degree of circular polarization, the absolute absorption cross sections and the component resolved magnetic moments of the $Fe_{0.50}Co_{0.48}V_{0.02}$ and Fe films as an example. This procedure may be easily adapted to other MCD and XAS experimental techniques.

We thank A. Gaupp for valuable discussions. This work is financially supported by the Swiss Federal Office for Education and Science and the European Community (contracts No BBW 97.0392 and FMGE-CT98-0105).

## Appendix

Data have been collected at several values of energy $E_n$, $n = 1 \dots N_E$, magnetization verse $\pm 1$, and for different incidence angles $\theta_j$, $j = 1 \dots N_a$.

As experimental standard deviations were not available, we performed a full-matrix non-linear unweighted[6] least-squares refinement for all spectra. This means minimizing the function

$$\chi^2 = 2\sum_{nj}\left(\left[\mathbb{T}_A^{\rm obs}\right]_{nj} - \left[\mathbb{T}_A^{\rm calc}\right]_{nj}\right)^2 + 2\sum_{nj}\left(\left[\mathbb{T}_D^{\rm obs}\right]_{nj} - \left[\mathbb{T}_D^{\rm calc}\right]_{nj}\right)^2.$$

In the expressions of the calculated transmittances $\mathbb{T}_D^{\rm calc}$, $\mathbb{T}_A^{\rm calc}$ (*cf.* Eqs. (7,8)) $\mu r$ and $\Delta\mu r$ are substituted by

$$\mu r = \beta_1(E_n) + \sum_{i=1}^{2}\tilde{\mathfrak{F}}_i(E_n)$$
$$\Delta\mu r = \beta_2(E_n) + \sum_{i=3}^{4}\tilde{\mathfrak{F}}_i(E_n)$$

with the Fano profiles $\tilde{\mathfrak{F}}_i(E)$ introduced in Section 3.2 (*cf.* Eq. (12)), $\beta_1, \beta_2$ contain all background terms.

In order to determine the refined parameters reliably, their number should be significantly smaller than the number of observations and the correlations should be as small as possible. For the Fe film $N_{\rm obs} : N_{\rm param} \approx 50 : 1$, for the $Fe_{0.50}Co_{0.48}V_{0.02}$ film $N_{\rm obs} : N_{\rm param} \approx 54 : 1$.

The program is a Fortran90 code by the authors. Different minimization algorithms are employed in succession. They all employ explicit evaluations of the function $\chi^2$ and its gradient $\nabla\chi^2$ with respect to the free parameters. Second derivatives were approximated by finite differences. At the end of the minimization we calculated the parameters' standard deviations by estimating the variance-covariance matrix $\mathsf{V}$ as $\mathsf{V} = {\rm GoF}\left[\mathsf{J}\mathsf{J}^T\right]^{-1}$, where $\mathsf{J}$ is the explicitly calculated Jacobian matrix of the calculated transmittances with respect to the parameters ($\mathsf{J}^T$ its transpose) and ${\rm GoF} = \chi^2/(N_{\rm obs} - N_{\rm param})$ is the goodness-of-fit. The variance-covariance matrix $\mathsf{V} = v_{ij}$ is defined as $v_{ij} = S_i S_j C_{ij}$, where $S_i$, $S_j$ are the standard deviations of the $i$- and $j$–th fitted parameter and $C_{ij}$ the relevant correlation coefficient ($C_{ii} = 1$ by definition). The final correlation coefficients turned out to be acceptably small. The standard deviations of the refined parameters can be obtained from the diagonal elements $v_{ii} = S_i^2$.

For the calculation of the magnetic moments (Eqs. (9, 10)) and relevant standard deviations, we also used the full $\mathsf{V}$ matrix. The standard deviation $S_f$ of a function $f(\boldsymbol{p})$ of the fitted parameters $\boldsymbol{p} = (p_1, ..., p_N)$ can be evaluated as $S_f = \left[\nabla_{\boldsymbol{p}} f \cdot \mathsf{V}\nabla_{\boldsymbol{p}} f\right]^{1/2}$.

[6] This corresponds to assuming for all the observed transmittances normally distributed errors with constant standard deviations. The normal distribution of errors was verified by repeated measurement of the transmitted intensity in the experimental energy range.

## References

1. B.T. Thole, P. Carra, F. Sette, G. van der Laan, Phys. Rev. Lett. **61**, 1943 (1992).
2. P. Carra, B.T. Thole, M. Altarelli, X.-D. Wang, Phys. Rev. Lett. **70**, 694 (1993).
3. R. Nakajima, J. Stöhr, Y.U. Idzerda, Phys. Rev. B **59**, 6421 (1999).
4. Y.U. Idzerda, C.T. Chen, H.-J. Lin, G. Meigs, G.H. Ho, C.-C. Kao, Nucl. Instr. Methods Phys. Res. A **347**, 134 (1994).
5. E. Stern, K. Kim, Phys. Rev. B **23**, 3781 (1981).
6. M.R. Weiss, K.J.S. Sawhney, R. Follath, H.-Ch Mertins, F. Schäfers, W. Frentrup, A. Gaupp, M. Scheer, J. Bahrdt, F. Senf, W. Gudat, *Synchrotron Radiation Instrumentation: 11th US National Conference*, edited by P. Pianetta *et al.* (American Institute of Physics, 2000) p. 134.
7. F. Schäfers, H.-Ch. Mertins, A. Gaupp, W. Gudat, M. Mertin, I. Packe, F. Schmolla, S. di Fonzo, G. Soullié, W. Jark, R. Walker, X. Le Cann, R. Nyholm, M. Eriksson, Applied Optics **38** 4074 (1990).
8. M. Born, E. Wolf, *Principles of Optics* (Pergamon Press, London 1956).
9. C.T. Chen, Y.U. Idzerda, H.-J. Lin, N.V. Smith, G. Meigs, E. Chaban, G.H. Ho, E. Pellegrin, F. Sette, Phys. Rev. Lett. **75**, 152 (1995).
10. U. Fano, Phys. Rev. **124**, 1866 (1961).
11. M. Domke, K. Schulz, G. Remmers, G. Kaindl, D. Wintgen, Phys. Rev. A **53**, 1424 (1996).
12. B.W. Shore , Phys. Rev. **171**, 43 (1968).
13. D.W. Lindle, T.A. Ferrett, U. Becker, P.H. Kobrin, C.W. Truesdale, H.G. Kerkhoff, D.A. Shirley, Phys. Rev. A **31**, 714 (1985).

14. M.B. Stearns, *Magnetic Properties of 3d, 4th and 5th Elements, Alloys and Compounds*, Vol. III/19a of *Landolt-Börnstein, New Series*, edited by K.-H. Hellwege, O. Madelung (Springer, Berlin, 1984).
15. R. Richter, H. Eschrig, J. Phys. F **18**, 1813 (1988).
16. H. Ebert, M. Battocletti, Solid State Commun. **98**, 785 (1996).
17. P. Söderlind, O. Eriksson, B. Johansson, R.C. Albers, A.M. Boring, Phys. Rev. B **45**, 12911 (1992).
18. O. Eriksson, B. Johansson, R.C. Albers, A.M. Boring, M.S.S. Brooks, Phys. Rev. B **42**, 2707 (1990).
19. Y.U. Idzerda, C.J. Gutierrez, L.H. Tjeng, H.-J. Lin, G. Meigs, C.T. Chen, J. Magn. Magn. Mater. **127**, 109 (1993).
20. S. Pizzini, A. Fontaine, E. Dartyge, C. Giorgetti, F. Baudelet, J.P. Kappler, P. Boher, F. Giron, Phys. Rev. B **50**, 3779 (1994).
21. M. Tischer, O. Hjortstam, D. Anvanitis, J. Hunter Dunn, F. May, K. Baberschke, J. Trygg, J.M. Wills, B. Johansson, O. Eriksson, Phys. Rev. Lett. **75**, 1602 (1995).
22. G. van der Laan, J. Phys. Cond. Matt. **9**, L259 (1997).